J Fluoresc (2016) 26:2177–2185
DOI 10.1007/s10895-016-1913-1

ORIGINAL ARTICLE

Highly Selective Sensing of Li^+ in H_2O/CH_3CN via Fluorescence 'Turn-on' Response of a Coumarin-Indole Linked Dyad: an Experimental and Theoretical Study

Santosh Kumari[1] · Sunita Joshi[2] · Amrit Sarmah[3] · Debi Pant[4] · Rajeev Sakhuja[1]

Received: 30 June 2016 / Accepted: 16 August 2016 / Published online: 27 August 2016

Abstract A coumarin-indole dyad, *N*-((7-hydroxy-2-oxo-2*H*-chromen-4-yl)methyl)-1*H*-indole-2-carboxamide has been synthesized and characterized by ^{1}H-NMR and ^{13}C-NMR. Effect of various metal ions on fluorescent behavior was also studied. The synthesized compound showed remarkable specificity towards Li^+ in organo-aqueous medium over other metal ions. Coordination of the compound with Li^+ induces a turn-on fluorescence response. The sensor exhibited good binding constant and low detection limit towards Li^+. Experimental results have been verified with Density Functional Theory and Time Dependent Density Functional Theory calculations.

Keywords Coumarin · Indole · Fluorescence · Sensor · Lithium · DFT

Introduction

Due to the importance of metal ions in various science sub-disciplines, great attention has been laid down towards developing newer molecules capable of sensing different metal ions in solution phase [1–6]. Among the metal ions, lithium ion is one the most biologically important alkali metal cation. Lithium-containing drug preparations are frequently used in clinical applications especially for the treatment of manic-depressive psychosis [7–10], [11]. Lithium also finds its use in treatment of skin diseases such as dermatitis and autoimmune and immunological diseases. In many cases, patients are required to take the drug over periods of several months or even years. The concentration of lithium ions in blood serum after drug intake varies from person to person and needs to be monitored in the individual patient routinely. Therefore, the reliable determination of the lithium ion concentration levels in blood samples is important for successful and safe therapeutic applications, since too low levels show no effect at all and an overdose of lithium can lead to life-threatening toxic effects. From the reported studies concentration of lithium ion in serum during the treatment should be within the narrow range of 0.6 and 1.2 mM [12, 13].

Many analytical techniques, such as ion selective electrodes [14, 15], colorimetric sensors [16, 17], voltammetry [18], atomic absorption and emission spectrometry [19, 20], chromatography [21] and inductively coupled plasma mass spectroscopy [22] have been used to determine the presence of metal ions in different samples. Among the various detection methods, fluorescence sensing [23–32] has become the most useful and popular technique in clinical, biology and environmental chemistry due to its non-destructive nature, high selectivity and sensitivity, real-time response and possible naked eye detection. Coumarin has been efficiently used as a fluorophore due to its excellent photo-physical properties such as great fluorescent intensity, high quantum yield, high photostability, biological stability and non-toxicity [33–35]. A number of examples of coumarin-based fluorescent probes are reported for sensing of different cations such as Fe^{3+}, Zn^{2+}, Cu^{2+}, Ni^{2+} and Hg^{2+} during the last decade [33–38]. Although

✉ Rajeev Sakhuja
sakhuja.rajeev@gmail.com

[1] Department of Chemistry, Birla Institute of Technology and Science, Pilani, Rajasthan 333 031, India

[2] Department of Pathophysiology, Charles University, Prague, Czech Republic

[3] Department of Chemistry, Ben-Gurion University, Negev, Israel

[4] Department of Physics, Birla Institute of Technology and Science, Pilani, Rajasthan 333031, India

several lithium sensors are known [39–41], however, very few reports on the development of fluorescent chemosensors for selective recognition of lithium ion in organic solvents have appeared [42–47]. One such example was recently reported by Sakai and Akutagawa, whereby quinoxalinone based fluorescent probe senses the cation ($M^+ = Li^+$ and Na^+) and anion ($X^- = F^-$, Cl^-, Br^-, and CH_3COO^-) in organic solvents [48]. However, selectively detecting Li^+ at low concentrations in aqueous medium by fluorescent chemosensors remains a appealing and necessary field of research [49]. In continuation of our [50, 51] effort on the the synthesis of coumarin based chemosensors, we report the synthesis of new coumarin-indole dyad based on a 'fluorophore–spacer–receptor' model, where the fluorescence emission at the coumarin site is modulated by Li^+ recognition at the indolic site. This resulted in efficient selective sensing of Li^+ which usually results in the suppression of photoinduced electron transfer (PET) quenching operating between the two moieties.

Experimental

Materials and Methods

All the chemicals were purchased from Sigma-Aldich, Alfa Aesar, and Spectrochem India Pvt. Ltd. and used without further purification. The solvents (HPLC grade) used were purchased from Merck (India) and were distilled and dried before use. Absorption spectra were taken using dual beam Thermo Evolution 201 UV/Vis/NIR spectrophotometer and fluorescence spectra were recorded using a Shimadzu RF-5301PC spectrofluorometer. The data were analyzed using related software. The concentration of compound in all the solutions prepared was 10^{-4} M. Nuclear Magnetic Resonance (NMR) spectra were recorded on Bruker 400 spectrometer. All ^{1}H NMR experiments were reported with TMS as an standard in δ units, parts per million (ppm), and were measured relative to residual DMSO (2.5 ppm) in the deuterated solvent. ^{13}C NMR spectra were reported in ppm relative to ppm [d_6] DMSO (39.5 ppm). All coupling constants J were reported in Hz. The following abbreviations were used to describe peak splitting patterns when appropriate: s = singlet, d = doublet, t = triplet, dd = doublet of doublet, m = multiplet and br s = broad singlet. Melting points were determined on a capillary point apparatus equipped with a digital thermometer. Mass spectra were recorded on Waters Synapt G2 high detection mass spectrometer at Core Instrumentation Centre, University of Mysore.

Synthesis of *N*-((7-hydroxy-2-oxo-2*H*-chromen-4-yl) methyl)-1*H*-indole-2-carboxamide (6)

To the stirred solution of **4** (0.300 g, 1.5 mmol, 1 eq.) in DMF, triethyl amine (2.5 eq.) was added drop-wise at 0 °C and subsequently EDC.HCl (0.429 g, 2.2 mmol, 1.5 eq.) and HOBt (0.243 g, 3.7 mmol, 1.2 eq.) was added and the reaction mixture was stirred for 20 min. at 0 °C. Later 1*H*-indole-2-carboxylic acid (0.303 g, 1.8 mmol, 1.2 eq.) was added and the reaction was stirred at room temperature for 6 h. The completion of the reaction was monitored by TLC. After the completion of the reaction, crushed ice was added that resulted in the precipitation of the product **6**, which was filtrated, washed with cold water and re-crystallized from ethanol. Yield: 0.235 g, 90 %; white solid; mp: 232–234 °C; ^{1}H NMR (400 MHz, DMSO-d_6) δ 12.11 (s, 1H), 9.47 (t, J = 5.6 Hz, 1H), 7.65 (t, J = 8.2 Hz, 2H), 7.47 (d, J = 8.2 Hz, 1H), 7.25 (s, 1H), 7.23–7.18 (m, 1H), 7.05 (s, 1H), 6.77 (dd, J = 8.8, 2.2 Hz, 1H), 6.68 (d, J = 2.2 Hz, 1H), 5.93 (s, 1H), 4.67 (d, J = 5.3 Hz, 2H); ^{13}C NMR

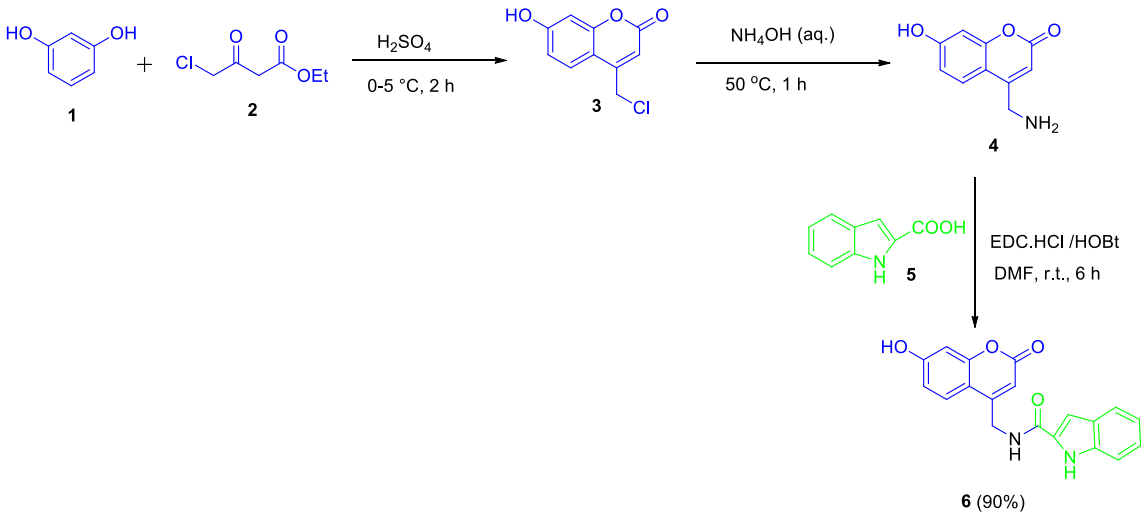

Scheme 1 Synthesis of coumarin-Indole Dyad (**6**)

(101 MHz DMSO-d_6) δ 166.0, 161.9, 161.4, 156.1, 154.4, 137.2, 131.7, 127.5, 125.8, 124.0, 122.1, 120.3, 115.0, 112.9, 108.4, 106.0, 104.0, 103.1, 24.8; HRMS: Chemical formula for $C_{19}H_{15}N_2O_4$; calcd 335.1024 $[M + H]^+$; found 335.1039$[M + H]^+$.

General Procedure for UV/Fluorescence Measurements

UV/Fluorescence measurements were carried in CH_3CN:water (3:7) with different Metal ions (5 eq.) keeping the concentration of compound **6** at 10^{-4} M. UV/Fluorescence titrations were carried in CH_3CN:water (3:7) with gradual increase in the concentration of Li^+ (0 to 100 μM) in a micro quartz cuvette, For each addition, at least three UV/fluorescence spectrums were recorded at 298 K to obtain concordant value. The λ_{ex} was chosen 340 nm for compound **6**, with 3 nm slit width.

Procedure for Quantum Yield of Calculation

The fluorescence quantum yield was determined by using quinine sulfate in 0.1 M sulfuric acid (Φ = 0.55) as the standard reference [52] The quantum yield is calculated using the following equation: [53]

$$\varphi_s = \varphi_r \frac{F_s A_r \eta_s^2}{F_r A_s \eta_r^2}$$

where A_r and A_s are the absorbance of the 'reference standard' and 'sample' respectively at the excitation wavelength, F_r and F_s are the relative integrated fluorescent intensities (area under the fluorescence curve, peak area) of the reference and samples respectively. η_r and η_s are respectively the refractive indices of the solvents in which the reference standard and samples are prepared.

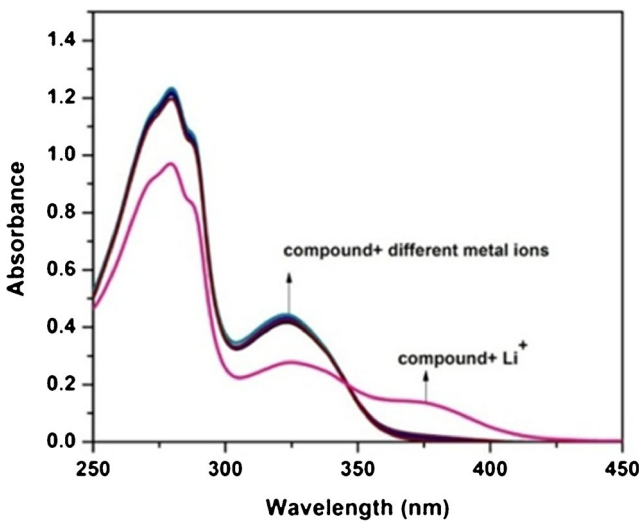

Fig. 1 UV–visible spectrum of **6** (10^{-4} M) upon addition of 5 equiv. of Li^+ and other metal ions

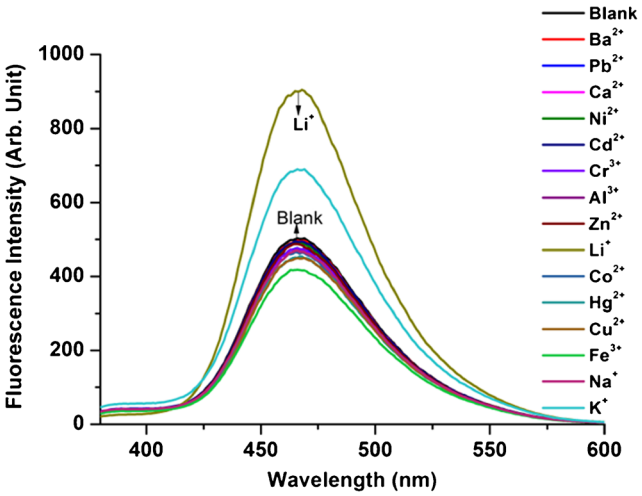

Fig. 2 Fluorescence spectra of **6** (10^{-4} M) upon addition of metal ions: Blank, Ba^{2+}, Pb^{2+}, Ca^{2+}, Ni^{2+}, Cd^{2+}, Cr^{3+}, Al^{3+}, Zn^{2+}, Li^+, Co^{2+}, Hg^{2+}, Cu^{2+}, Fe^{3+}, Na^+ and K^+ (5 equiv.) in H_2O/CH_3CN. [λ_{ex} = 340 nm & λ_{em} = 465 nm]

Computational Calculations

All the Density Functional Theory (DFT) based calculations are performed using the Gaussian09 (G09) [54] program package. Geometry of the compound **6** along with its different analogues (after attachment of Li^+) are fully optimized at B3LYP/6-31G(d,p) level [55, 56]. The minimum energy of the optimized structures is ensured through frequency calculations. Absence of any negative frequencies indicates the global minima for the optimized geometry on potential energy surface. To provide some details insights to the different electronic transitions associated with UV-VIS spectrum, Time Dependent Density Functional Theory (TD-DFT) [57, 58]

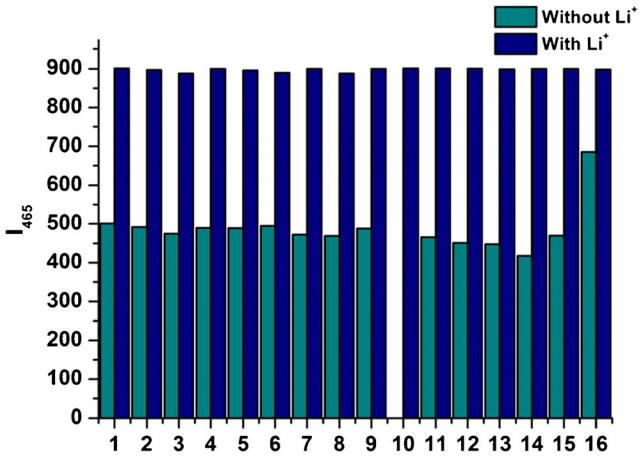

Fig. 3 Column diagrams of the fluorescence intensity of compound + Metal ions at 465 nm. Dark cyan bars represent the addition of various metal ions to the blank solution and navy blue bars represent the subsequent addition of Li^+ (5 equiv.) to the above solutions (compound + M^{n+} + Li^+); From left to right (i) Blank; (ii) Ba^{2+}; (iii) Pb^{2+}; (iv) Ca^{2+}; (v) Ni^{2+}; (vi) Cd^{2+}; (vii) Cr^{3+}; (viii) Al^{3+}; (ix) Zn^{2+}; (x) Li^+; (xi) Co^{2+}; (xii) Hg^{2+}; (xiii) Cu^{2+}; (xiv) Fe^{3+}; (xv) Na^+; (xvi) K^+

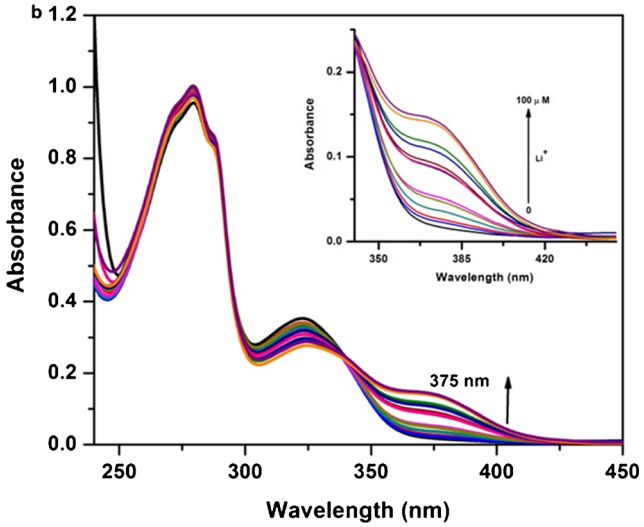

Fig. 4 UV–visible titration profile of compound **6** in H_2O:CH_3CN (7:3, *v*/v) solution upon concomitant additions of Li^+ ion (0 to 100 μμ) inset – absorption changes at 375 nm

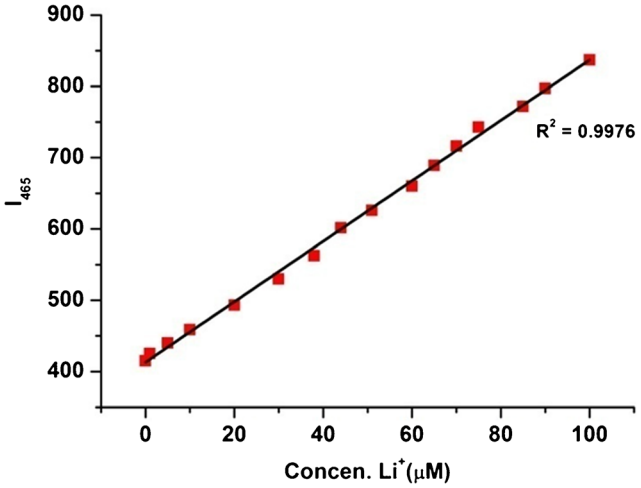

Fig. 6 The plot of I_{465} vs. the concentration of Li^+

calculations are also done at the same level of theory and basis sets, i.e., B3LYP/6-31G(d,p). The solvent effect of water has been incorporated in entire calculations through Self-Consistent Reaction Field (SCRF) [59] formalism using IEF-PCM model [60] as implemented in Gaussian09.

Results and Discussion

The newly synthesized fluorescent coumarin-indole dyad was synthesized as shown in Scheme 1. Commercially available resorcinol (**1**) on reaction with ethyl chloroacetoacetate (2) in presence of sulfuric acid at 0–5 °C afforded 4-(chloromethyl)-7-hydroxy-2*H*-chromen-2-one [61] (**3**), which on reaction with 25 % ammonium hydroxide at 50 °C for 1 h yielded 7-hydroxy-4-(aminomethyl)coumarin [62] (**4**) in 80 % yield. The coupling of **4** with 1*H*-indole-2-carboxylic acid (**5**) using EDC.HCl/HOBt in DMF at room temperature for 6 h yielded coumarin-indole dyad linked via methylene bridge (**6**) in 92 % yield (Scheme 1). The structure of **6** was confirmed by ^1H NMR, ^{13}C NMR, and high resolution mass spectrometry.

UV − vis absorption and steady state fluorescence emission of **6** was measured in organo-aqueous solution in the absence and presence of metal ions at room temperature. In order to choose an appropriate solvent, selectivity test was performed with a number of solvent systems including H_2O/CH_3CN, H_2O/THF, H_2O/DMSO. We established that compound **6** showed good fluorescence efficiency in acetonitrile than other solvents studied (H_2O/THF, H_2O/DMSO). The binding capacity of the coumarin-Indole Dyad (compound **6**) towards various metal ions (5 equiv.) such as Ba^{2+}, Pb^{2+}, Ca^{2+}, Ni^{2+}, Cd^{2+}, Cr^{3+}, Al^{3+}, Zn^{2+}, Li^+, Co^{2+}, Hg^{2+}, Cu^{2+}, Fe^{3+}, Na^+ and K^+ was measured by UV-vis absorption studies. UV-vis spectrum of compound **6** exhibited absorption bands at 322 nm and 280 nm in H_2O/CH_3CN (7:3, *v*/v) ratio. When Li^+ was added to the compound **6**, a new red shifted band emerged at

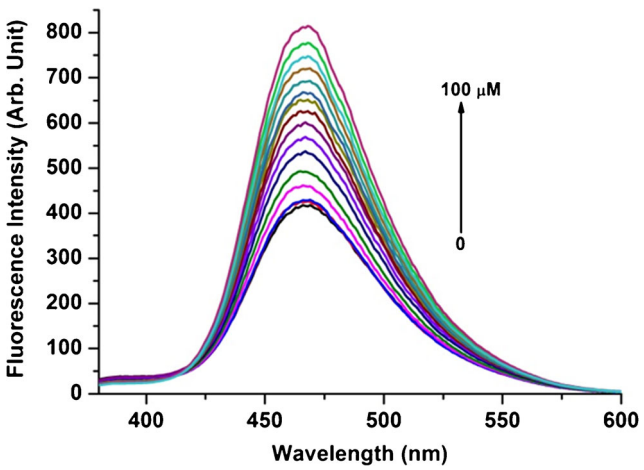

Fig. 5 Fluorescence spectra of compound **6** with addition of various concentrations of Li^+ in H_2O/CH_3CN (λ_{ex} = 340 nm)

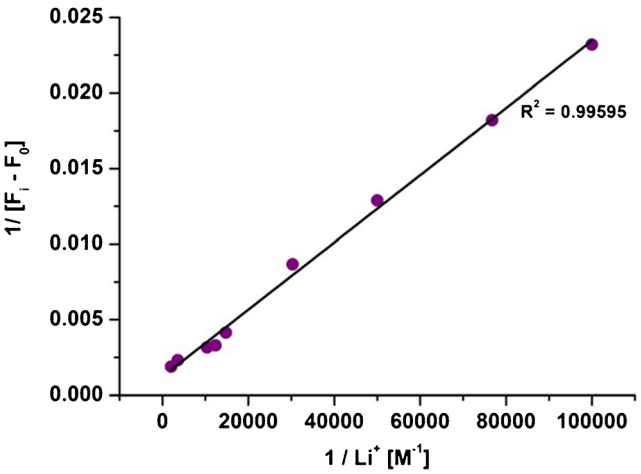

Fig. 7 Benesi-Hildebrand plot for compound at various concentrations of Li^+

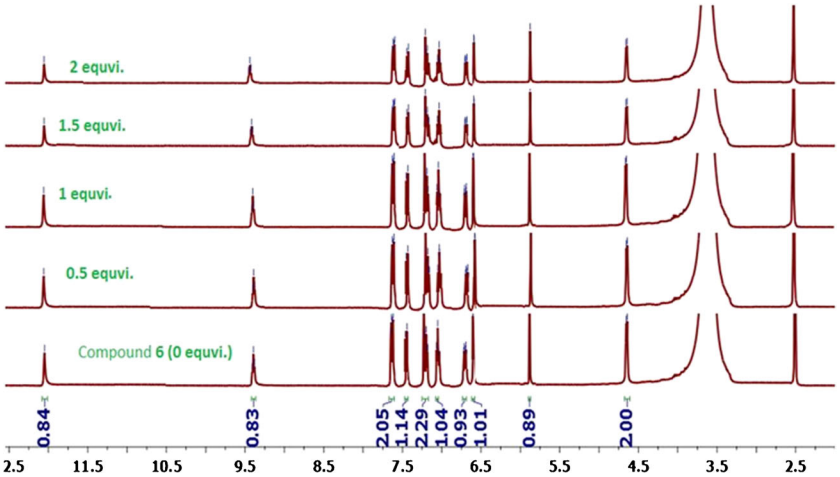

Fig. 8 ^{1}H NMR of compound **6** (bottom) in the presence of 0.5–2 equiv. of Li + in DMSO-d_6

375 nm (Fig. 1). This could be due to delocalization of electrons on formation of complex between Li^+ and compound **6**. Moreover, the red-shift can also be explained due to the intramolecular charge transfer (ICT) process and the lowering of the band gap between HOMO and LUMO on complexation with Li^+. Importantly, no distinguishable spectral change in the UV-vis spectrum of compound **6** was observed in the presence of other tested metal ions.

To further explore sensing behavior of **6**, fluorescence experiments were carried out by mixing it with different metal ions (5 equiv.) namely Ba^{2+}, Pb^{2+}, Ca^{2+}, Ni^{2+}, Cd^{2+}, Cr^{3+}, Al^{3+}, Zn^{2+}, Li^+, Co^{2+}, Hg^{2+}, Cu^{2+} and Fe^{3+} in H_2O/CH_3CN (7:3, *v*/v) ratio. Compound **6** exhibited fluorescence maxima at 465 nm (λ_{ex} = 340 nm) in absence of metal ions with very low quantum yield (Φ = 0.129). Addition of Li^+ (5 equiv.) to the above solution shows an excellent fluorescence enhancement and an increase in quantum yield to 0.262, while metal ions Ba^{2+}, Pb^{2+}, Ca^{2+}, Ni^{2+}, Cd^{2+}, Cr^{3+}, Al^{3+}, Zn^{2+}, Co^{2+}, Hg^{2+}, Cu^{2+} and Fe^{3+} (5 equiv.) did not affect the fluorescence spectra of **6** studied (Fig. 2).

To evaluate the selectivity of compound **6** toward Li^+ ions over other metal ions, competitive fluorescence experiments of the Li^+ (5 equiv.) solutions mixed with other common interfering metal ions such as Ba^{2+}, Pb^{2+}, Ca^{2+}, Ni^{2+}, Cd^{2+}, Cr^{3+}, Al^{3+}, Zn^{2+}, Co^{2+}, Hg^{2+}, Cu^{2+}, Fe^{3+}, Na^+ and K^+ (5 equiv.) were carried out. In Fig. 3 the navy blue bars represent the intensity of the emitted radiation in the presence of Li^+ ions in solution together with individual metal ions such as

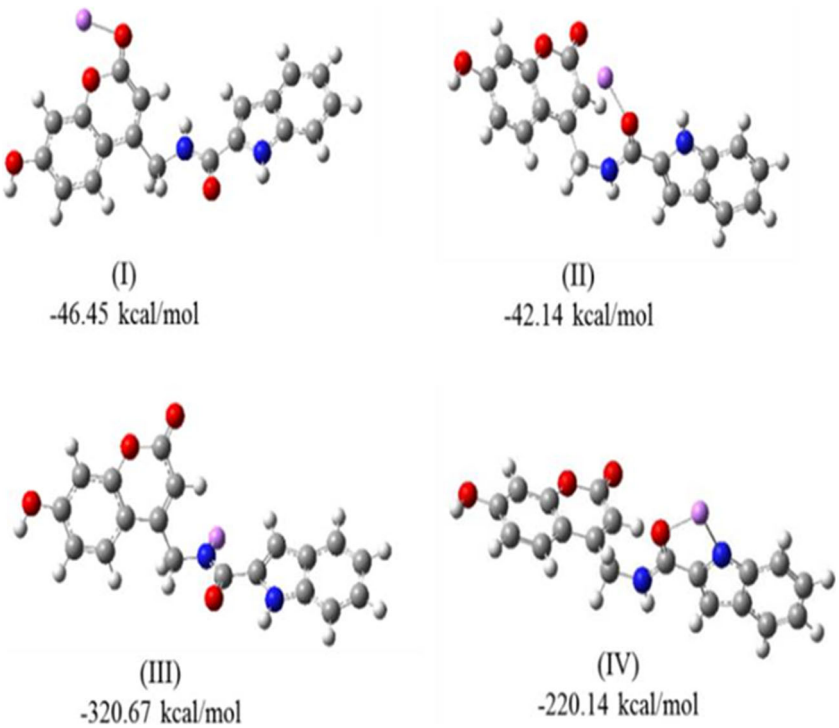

Fig. 9 Optimized structure of the compound after complexation with Li^+ and their corresponding binding energy values. Hydrogen atoms are omitted for clarity. Binding Energy is calculated as $BE = E_{complex} - (E_{compound} + E_{Li})$ $BE = E_{complex} - (E_{compound} + E_{Li})$

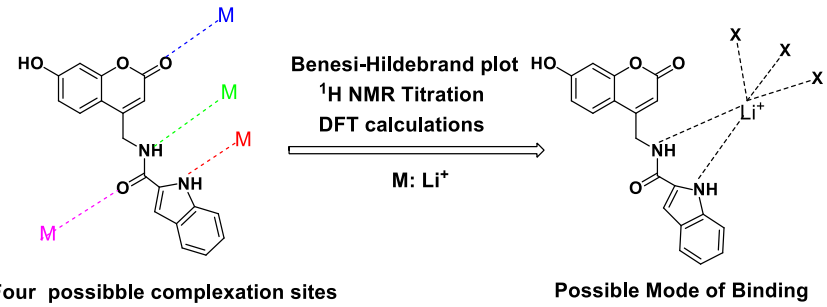

Fig. 10 Proposed binding site for compound **6** + Li^+

Ba^{2+}, Pb^{2+}, Ca^{2+}, Ni^{2+}, Cd^{2+}, Cr^{3+}, Al^{3+}, Zn^{2+}, Li^+, Co^{2+}, Hg^{2+}, Cu^{2+}, Fe^{3+}, Na^+ and K^+ that shows high impact on the emission intensity when compared to the dark cyan bars which correspond to the emission intensity of a solution of the same metal ion in the absence of Li^+. The results showed that, the fluorescence enhancement of **6** was not affected by the competing ions. Therefore compound **6** can be used as highly selective sensor for detection of Li^+ ions in the presence of other common metal ions.

The absorption titration was next performed with an incremental addition of Li^+ (Fig. 4) that caused a progressive increase in the absorption band around 375 nm suggesting that the compound has high sensitivity toward Li^+ metal ion. The spectral changes with the formation of isosbetic point at 340 nm indicate the formation of single complex species between sensor and Li^+.

The fluorescence titration of compound **6** was performed in the presence of various concentrations of Li^+ in H_2O/CH_3CN 7:3 (v/v) in Fig. 5. Upon addition of increasing amount of Li^+ leads to a continuous fluorescence enhancement around 465 nm.

By using the above mentioned titration results, the detection limit for Li^+ ion was calculated. The emission intensity of compound **6** without Li^+ was measured by ten times and standard deviation of blank measurements was determined. The fluorescence intensity increased linearly with an increase in the concentration of Li^+ (Fig. 6). The limit of detection was measured [63], [64, 65] to be 37.1 nM for compound **6**, based on 3σ/m, where σ corresponds to the standard deviation of the blank measurements, and m is the slope in the plot of the intensity versus the sample concentration (Fig. 6). Therefore the sensor is responsible for nanomolar determination of lithium in various samples.

For investigating the binding stoichiometry and the determining the association constant, Benesi-Hildebrand plot [66] was constructed. The linearity of Benesi-Hildebrand plot (Fig. 7) between $1/(F_i - F_0)$ against $1/[Li^+]$ indicates the 1:1 stoichiometry between sensor and Li^+ ions. The association constant was found to be $K_a = 5.5 \times 10^3\ M^{-1}$ for compound as obtained from Benesi-Hildebrand plot. The high value of association constant K_a indicates that a strong complex formation takes place between metal ion (Li^+) and ligand (**6**).

We next aim to understand the most probable site of coordination for the Li^+ that might be responsible for the "turn-on" fluorescence behaviour of compound **6**. Different binding sites are available in the compound **6** where the metal ion (Li^+) could bind, which includes (i) the carbonyl oxygen of coumarin moiety, (ii) the carbonyl oxygen of amide linkage, (iii) amidic N-H, and (iv) indolic N-H. To elucidate the most prominent binding site in compound **6** for Li^+, ^1H NMR titration experiments were carried out in DMSO-d_6 (Fig. 8). The addition of 1 equivalent of lithium salt to the solution of compound **6** in DMSO-d_6 led to slight down-field shifts in the position of indolic NH (0.007 ppm) and amidic NH (0.008 ppm), thereby indicating the binding of Li^+ to indolic and amidic NH. No further change in the ^1H NMR of compound **6** was observed upon addition of more than 1 equiv. of Li^+, thereby confirming 1:1 stoichiometry, as earlier suggested by Benesi-Hildebrand plot. The results suggested the binding of compound **6** to Li^+ by a rigid conjugation system through interactions with indolic NH and amide proton [67].

Binding energy calculations are performed to determine the most possible binding site of Li^+ in the compound. The binding energy values corresponding to the binding of Li^+ at the four possible binding sites (mentioned above) were computed

Table 1 Computed vertical electronic transitions with oscillator strength (*f*) and other relevant parameters for the compound and Li-compound complex. Calculated at TD-B3LYP/ 6-31G(d,p)/scrf = (iefpcm, solvent = water) level

System	Origin	CI Contribution	λ nm	E (eV)	*F*	*Assign*
Compound	S_0 to S_1	HOMO → LUMO(98 %)	330	3.74	0.0017	(n → π*)
	S_0 to S_2	HOMO-1 → LUMO(94 %)	300	4.12	0.423	(π → π*)
	S_0 to S_5	HOMO-2 → LUMO(82 %)	277	4.00	0.4898	(π → π*)
Li-Complex	S_0 to S_1	HOMO → LUMO(98 %)	378	3.28	0.0117	(π → π*)

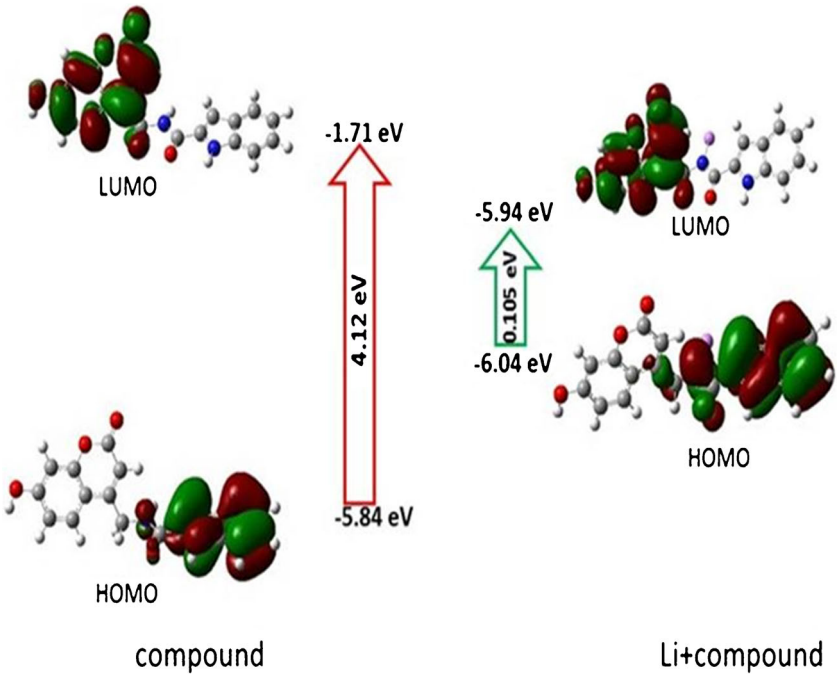

Fig. 11 Possible HOMO-LUMO transitions for the compound and its Li-complex

and the values are reported below along with the optimized geometries (Fig. 9).

From the computed BE values, it's clear that the attachment of Li^+ on the amidic NH is thermodynamically most preferable (BE = −320.67 kcal/mol). Indeed, the indolic NH (BE = −220.14 kcal/mol) also appears to be a potential binding site and might be stabilized by some kind of weak interaction (bridging) with the neighboring oxygen of C = O group. However, the computed bond distance values show that the Li is relatively closer to nitrogen compared to the oxygen atom. The Li-N bond length is 1.69 A^0 whereas the Li-O is 1.98 A^0. So, it can be argued that the bonding between Li-O rather appears to be a weak interaction. It is worth mentioning here that the higher binding affinity of Li^+ for amidic NH is also evident from the experimental spectroscopic data. Based on the ^1H NMR titration study, Benesi-Hildebrand plot and DFT calculation results, the possible structure of compound **6** + Li^+ is proposed in Fig. 10.

TD-DFT calculations are performed to understand the visible changes in the nature of electronic excitations associated with the UV-vis spectrum of the compound before and after the attachment of Li^+. The ground state optimized geometries are considered as the starting orientation for TD-DFT calculations. The findings of TD-DFT calculation are reported in Table 1. The Frontier Molecular Orbital (FMO) picture of the compound along with its Li analogue is provided in Fig. 11. The two intense band in the UV-vis spectrum of the compound **6** at 300 nm (f = 0.423) (λ_{exp} = 322 nm) and 277 nm (f = 0.4898) (λ_{exp} = 280 nm) results from the $\pi \rightarrow \pi^*$ type of electronic transitions (Table 1).

Table 2 A comparative study with previous literature reports

Publication	Material used	Detection Limit	Medium Used
Present manuscript	Coumarin derivative	37.1 nM	H_2O/ CH_3CN (*v*/v = 7:3)
Tetrahedron Lett. 2002, 43, 4989	diaza-9-crown-3 derivative	-	CH_3CN
J. Photochem. Photobiol. A 2004, 162,289	N-(9-methylanthracene)-25, 27-bis(1-propyloxy)-4-tert-butylcalix [4]arene-azacrown-3	3.2 μM	Dichloromethane/THF (v/v = 75:25)
Dyes Pigments 1999, 43 , 21	squarylium dye	-	CH_2Cl_2/CH_3CN (v:v /1:4)
Tetrahedron 2004, 60 5799	diaza-9-crown-3 derivatives	-	CH_3CN
Organic Lett. 2004, 6, 4599	1-(9-anthryl)-4-ferrocenyl-2-aza-1,3-butadien		H_2O/ CH_3CN (v/v = 7:3)
RSC Adv. 2016, 6, 1792	Biginelli-based organic nanoparticles	122 nM	H_2O
Talanta 1998,46, 703	Porphyrin	<1 ppm	H_2O
Anal. Chem. 2007, 79, 1237	Polymer based fluoroionophore	0.6 mM	H_2O/ CH_3OH (v/v = 99:1)
Dyes and Pigments 2009, 82, 336	Polyamidoamine dendrimer	-	DMF + NaOH

This is basically an intramolecular charge transfer (ICT) process (from the orientation of FMOs). With the addition of Li^+ to the compound **6**, a red shifted absorption band is appeared at 378 nm (λ_{exp} = 375 nm) with a comparatively low oscillator strength nm (f = 0.0117). Subsequently the TD-DFT based computations correlate well with the experimental results. With the addition of Li^+, a significant decrease in the HOMO-LUMO gap is also observed for the compound (Fig. 11).

As observed above, the coumaryl-indole dyad sensor (**6**) showed an increase in fluorescence intensity when coordinated with Li^+ ion. The responsible phenomenon for enhancement of fluorescence intensity with the metal ion is due to inhibition of PET as previously reported [68–70]. In absence of Li^+, when the compound **6** is in turn off mode, the lone pair of electrons residing on amide nitrogen is exclusively delocalized in the coumarin ring which leads to non-radiative decay of the excited state and could be responsible for flourescence quenching. However, when compound **6** interacts with metal ion Li^+ it coordinates through amide–N and indolic-N moieties, which in turn introduces planarity and rigidity in the molecule that further inhibits the non-radiative decay of the excited state leading to increase in emission of compound [71–73].

Comparison with previously Reported Methods

The sensing ability of the present compound towards Li^+ ion was also compared with other reported in literature, which is given in (Table 2). It is evident, from the comparison, that the present compound is a simple sensor for Li^+ ion and its LOD is in nanomolar. The present method involves highly sensitive, selective method and avoids the need for sophisticated and costly instruments.

Conclusions

In summary, a new, efficient, highly sensitive and selective coumarin-indole dyad has been synthesized and characterized for efficient detection of Li^+ in organo-aqueous media. Moreover the rapid enhancement of fluorescence emission intensity on addition of Li^+ even in the presence of other metals also provides a wonderful detection technique for Li^+ detection. High association constant for complex ($K_a = 5.5 \times 10^3\ M^{-1}$, respectively) and detection limit in nanomolar range (37.1 nM) makes compounds **6** an excellent Li^+ sensor. The most probable binding site of complexing Li^+ have explained by ^1H NMR titration and DFT calculation. The spectral change by addition of Li^+ has been supported by TDDFT calculation.

Acknowledgments The authors acknowledge the Department of Science & Technology (DST), New Delhi, for research funding (SB/FT/CS-033/2012). SK is thankful to University Grants Commission (UGC), New Delhi for Senior Research Fellowship.

References

1. Bissel RA, de Silva AP, Gunaratne HQN, Lynch PLM, Maguire GEM, Sandanayake KRAS (1992) Chem Soc Rev 21:187–195.
2. de Silva AP, Gunaratne HQN, Gunnlaugsson T, Huxley AJM, McCoy CP, Rademacher JT, Rice TE (1997) Chem Rev 97:1515–1566.
3. Desvergne JP, Czarnik AW (1997) Fluorescent Chemosensors for Ion, Molecule Recognition; Eds. Kluwer Academic Publishers, Dordrecht, The Nederlands
4. Prodi L, Bolletta F, Montalti M, Zaccheroni N (2000) Coord Chem Rev 205:59–83
5. Valeur B, Leray I (2000) Coord Chem Rev 205:3–40
6. de Silva AP, Fox DB, Huxley AJM, Moody TS (2000) Coord Chem Rev 205:41–57
7. Bach RO (1985) Lithium-Current Applications in Science, Medicine and Technology. Wiley-Interscience, New York
8. Aurbach DJ (2000) Power Sources 89:206–218
9. Lantelme F, Groult H, Kumagni N (2000) Electrochem. Acta 45: 3171–3178
10. W. H. Meyer (1998) Adv Mater 10: 439–448.
11. Yin J, Hua Y, Yoon J (2015) Chem Soc Rev 44:4619–4644.
12. Jope RS (1999) Mol Psychiatry 4:117–128.
13. Manji HK, Potter WZ, Lenox RH (1995) Arch Gen Psychiatry 52: 531–543.
14. Gupta VK, Jain AK, Maheshwari G (2007) Talanta 72:1469–1473
15. Gupta VK, Goyal RN, Jain AK, Sharma RA (2009) Electrochim Acta 54:3218–3224.
16. Gupta VK, Singh AK, Ganjali MR, Norouzi P, Faridbod F, Mergu N (2013) Sens. Actuators B Chem 182:642–651
17. Chen S, Fang YM, Xiao Q, Li J, Li SB, Chen HJ, Sun JJ, Yang HH (2012) Analyst 137:2021–2023
18. Mohadesi A, Taher MA (2007) Talanta 72:95–100
19. Mashhadizadeh MH, Pesteh M, Talakesh M, Sheikhshoaie I, Ardakani MM, Karimi MA (2008) Spectrochim Acta B 63: 885–888.
20. Cassella RJ, Magalhaes OIB, Couto MT, Lima ELS, Neves MAFS, Coutinho FMB (2005) Talanta 67:121–128
21. Ali A, Shen H, Yin X (1998) Anal Chim Acta 369:215–223.
22. Ferreira SLC, Queiroz AS, Fernandes MS, dos Santos HC (2002) Spectrochim. Acta B 57:1939–1950
23. Li YP, Ming X, Zhang YH, Chang Z (2013) Inorg Chem Commun 33:6–9.
24. Chen CH, Liao DJ, Wan CF, Wu AT (2013) Analyst 138:2527–2530
25. Gupta VK, Singh AK, Mergu N (2014) Electrochim Acta 117:405–412.
26. Gupta VK, Singh AK, Kumawat LK (2014) Sens. Actuators B Chem. 195:98–108
27. Gupta VK, Mergu N, Singh AK (2014) Sens. Actuators B Chem. 202:674–682
28. Gupta VK, Mergu N, Kumawat LK, Singh AK (2015) Sens. Actuators B Chem. 207:216–223
29. Kim KB, You DM, Jeon JH, Yeon YH, Kim JH, Kim C (2014) Tetrahedron Lett 55:1347–1352.
30. Azadbakht R, Khanabadi J (2013) Tetrahedron 69:3206–3211
31. Chaoxia G, Xiaofeng Y, Xiangyong W, Meishan P, Guangyou Z (2013) New J Chem 37:4163–4169.

32. Zhou D, Sun C, Chen C, Cui X, Li W (2015) J Mol Struct 1079: 315–320.
33. Su Z, Chen K, Guo Y, Qi H, Yang X, Zhao M (2010) J Fluoresc 20: 851–856.
34. Ma Q, Zhang X, Zhao X, Jin Z, Mao G, Shen G, Yu R (2010) Anal Chim Acta 663:85–90.
35. Chattopadhyay N, Mallick A, Sengupta S (2006) J Photochem Photobiol A 177:55–60
36. Hyo SJ, Ji HH, Zee HK, Chul HK, Jong SK (2011) Org Lett 13: 5056–5059.
37. Kirubaharan CJ, Kalpana D, Lee YS (2012) Ind Eng Chem Res 51: 7441–7446.
38. Joshi S, Kumari S, Bhattacharjee R, Sarmah A, Sakhuja R, Pant DD (2015) Sens. Actuators B Chem. 220:1266–1278
39. Ciampolini M, Nardi N, Valtancoli B, Micheloni M (1992) Coord Chem Rev 120:223–236.
40. Kobiro K (1995) Coord Chem Rev 148:135–149
41. Formica M, Fusi V, Micheloni M, Pontellini R, Romani P (1999) Coord Chem Rev 184:347–363.
42. Cimpolini M, Formica M, Fusi V, Saint-Mauricec A, Micheloni M, Nardi N, Pontellini RR, Pina F, Romani P, Sabatini AM, Valtoncoli B (1999) Eur J Inorg Chem 1999:2261–2268
43. Obare SO, Murphy CJ (2001) Inorg Chem 40:6080–6082.
44. Gunnlaugsson T, Bichell B, Nolan C (2002) Tetrahedron Lett 43: 4989–4992.
45. Benco JS, Nienaber HA, McGimpsey WG (2004) J. Photochem. Photobiol. A 162:289–296
46. King SH, Han SK, Park SH, Yoon CM, Keum SR (1999) Dyes Pigments 43:21–25
47. Gunnlaugsson T, Bichell B, Nolan C (2004) Tetrahedron 60: 5799–5806
48. Nakane Y, Takeda T, Hoshino N, Sakai KI, Akutagawa T (2015) J Phys Chem A 119:6223–6231.
49. Bissell RA, de Silva AP, Gunaratne HQN, Lynch PLM, Maguire GEM, Sandanayake KRAS (1992) Chem Soc Rev 21:187–195.
50. Kumari S, Joshi S, SMA S, Agarwal D, Panda SS, Pant DD, Sakhuja R (2015) Aus. J Chem 68:1415–1426
51. Kumari S, Joshi S, Cordova-Sintjago TC, Pant DD, Sakhuja R (2016) Sens. Actuators B: Chem 229:599–608
52. Mishra H, Pant D, Pant TC, Tripathi HB (2006) J Photochem Photobiol A Chem 177:197–204
53. Ranjitha C, Vijayana KK, Praveena VK, Saleesh NS (2010) Spectrochim. Acta Part A 75:1610–1616
54. Frisch MJ (2009) Gaussian 09, Revision D.01, Gaussian, Inc., Wallingford CT
55. Becke AD (1993) J Chem Phys 98:5648–5652.
56. Lee C, Yang W, Parr RG (1988) Phys Rev B 37:785–789.
57. Stratmann RE, Scuseria GE, Frisch MJ (1998) J Chem Phys 109: 8218–8224
58. Casida M E, Jamorski C, Casida KC, Salahub DR (1998) J Chem Phys 108: 4439–4445.
59. Miertuš S, Scrocco E, Tomasi J (1981) Chem Phys 55:117–129.
60. Miertuš S, Tomasi J (1982) Chem Phys 65:239–241.
61. Lin W, Long L, Feng J, Wang B, Guo C (2007) Eur J Org Chem 26: 4301–4304
62. Onderwater RCA, Venhorst J, Commandeur JNM, Vermeulen NPE (1999) Chem Res Toxicol 12:555–559.
63. Zhang F, Wang L, Chang SH, Huang KL, Chi Y, Hung WY, Chen CM, Lee GH, Chou PT (2013) Dalton Trans 42:7111–7119.
64. Neupane LN, Kim JM, Lohani CR, Lee KH (2012) J Mater Chem 22: 4003–4008.
65. Yang MH, Thirupathi P, Lee KH (2011) Org Lett 13:5028–5031.
66. Benesi HA, Hilderbrand JH (1949) J Am Chem Soc 71:2703–2707.
67. Sun YL, Wu AT (2013) J Fluoresc 23: 629–634.
68. Bryan AJ, de Silva AP, de Silva SA, Rupasinghe RADD, Sandanayake KRAS (1989) Biosensors 4:169–179
69. Bissell RA, de Silva AP, Gunaratne HQN, Lynch PLM, Maguire GE M, Sandanayake KRAS (1992) Chem Soc Rev 21:187–195.
70. He H, Mortellaro MA, Leiner MJP, Young ST, Fraatz RJ, Tusa JK (2003) Anal Chem 75:549–555.
71. Suresh M, Mandal AK, Saha S, Suresh E, Mandoli A, Liddo RD, Parnigotto PP, Das A (2010) Org Lett 12: 5406–5409.
72. Yin S, Zhang J, Feng HK, Zhao Z, Xu L, Qiu H, Tang B (2012) Dyes Pigments 95:174–179.
73. Jayabharathi J, Thanikachalam V, Jayamoorthy K (2012) Spectrochim Acta A 95:143–147.